Journal of Statistical Physics, Vol. 27, No. 4, 1982

Critical Behavior of a KAM Surface: I. Empirical Results

Scott J. Shenker[1,2] **and Leo P. Kadanoff**[1]

Received July 20, 1981

Kolmogorov–Arnol'd–Moser (KAM) surfaces are studied in the context of a perturbed two-dimensional twist map. In particular, we ask how a KAM surface can disappear as the perturbation parameter is increased. Following Greene, we use cycles to numerically construct the KAM curve and discover that at the critical coupling it shows structure at all length scales. Aspects of this structure are fitted by a scaling analysis; critical indices and scaling functions are determined numerically. Some evidence is presented which suggests that the results are universal.

KEY WORDS: KAM surface; twist map; critical exponents; coupled oscillators.

1. INTRODUCTION

In recent years, it has become fashionable to utilize discrete maps in studying dynamical problems involving instability, noise, or stochasticity.[1-4] These discrete methods seem especially well suited to exploring the transition to chaotic behavior in simple dynamical systems.[5] Following the work of Greene,[6-9] we use two-dimensional, area-preserving maps to investigate a particular brand of chaotic transition: the destruction of KAM surfaces in conservative Hamiltonian systems with two degrees of freedom. Much of the preliminary material has been covered extensively in recent review articles[10-12] and will only be covered here briefly.

Supported in part by the Materials Research Laboratory Program of the National Science Foundation at the University of Chicago under grant No. NSF-MRL 7924007.

[1] The James Franck and Enrico Fermi Institutes of the University of Chicago, 5640 South Ellis Avenue, Chicago, Illinois 60637.

[2] Robert R. McCormick and National Science Foundation Fellow.

0022-4715/82/0400-0631$03.00/0

In integrable Hamiltonian systems with n degrees of freedom, all trajectories lie on invariant n-tori. The content of the theory developed by Kolmogorov, Arnol'd, and Moser (KAM)[13–15] is that most (in the sense of measure theory) of these invariant n-tori persist, albeit deformed, when a sufficiently small perturbation is added to the original Hamiltonian. These surviving invariant n-tori are called KAM surfaces. As the magnitude of the perturbation increases, fewer and fewer of the KAM surfaces remain. The question we address in this paper is how does a KAM surface disappear?

We study this question in the context of conservative and integrable Hamiltonian systems with two degrees of freedom. The dynamics of such a system is essentially that of two uncoupled oscillators. In action-angle coordinates I, J, θ, ϕ, the equations of motion are simply

$$\begin{aligned} I(t) &= I(0), \qquad J(t) = J(0) \\ \theta(t) &= \omega_1 t + \theta(0), \qquad \phi(t) = \omega_2 t + \phi(0) \end{aligned} \tag{1.1}$$

where the frequencies ω_1, ω_2 are functions of I and J. The problem can be made discrete by only considering the values I_n, θ_n of $I(t)$, $\theta(t)$ when $\phi(t) = n$ and working at one specified total energy E. (Here, and elsewhere in this paper, we identify ϕ with $\phi + 1$ in phase space and absorb all factors of 2π.) This generates a trivial recursion relation called the twist map

$$\begin{bmatrix} r_{n+1} \\ \theta_{n+1} \end{bmatrix} = \begin{bmatrix} r_n \\ \theta_n + r_n \end{bmatrix} = T_0 \begin{bmatrix} r_n \\ \theta_n \end{bmatrix} \tag{1.2}$$

where $r_n = \omega_1/\omega_2$, a function of I_n and E, is called the winding number.

This discrete map captures all of the essential physics of the integrable continuous system. Each initial condition $z_0 = (r_0, \theta_0)$ generates a series of points $z_1, z_2, \ldots$ which is a discrete representation of a continuous dynamical trajectory. The qualitative nature of the trajectory is determined completely by the winding number. If $r_0 = P/Q$ for P, Q relatively prime integers, then the resulting series of points is a periodic Q-cycle with $r_Q = r_0$, $\theta_Q = \theta_0 + P$. If the winding number is irrational then the resulting points never repeat but continue to fill densely the line $r = r_0$ in the r, θ plane. This invariant curve $r = r_0$ is merely the discrete representation of an invariant 2-torus in phase space.

If we add a perturbation to the Hamiltonian to generate a nonintegrable system, that will have the effect of perturbing the twist map. Since we are restricting ourselves to conservative systems, the map must remain area-preserving. A new kind of motion emerges in the continuous system, one which appears to cover a whole three-dimensional region in the four-dimensional phase space. Correspondingly, the discrete map shows sequences of points $\{z_n\}$ that never repeat and which do not lie on any

smooth curve. These kinds of sequences are called chaotic trajectories. They are associated with invariant tori which have been destroyed by the perturbation.

In this paper, we study one particular family of perturbed twist maps, called the Chirikov–Taylor[12,16] map

$$\begin{bmatrix} r_{n+1} \\ \theta_{n+1} \end{bmatrix} = \begin{bmatrix} r_n + kg(\theta_n) \\ \theta_n + r_n + kg(\theta_n) \end{bmatrix} = T_k \begin{bmatrix} r_n \\ \theta_n \end{bmatrix} \tag{1.3}$$

where, in the standard form, $g(\theta) = -(1/2\pi)\sin 2\pi\theta$. The Moser twist theorem[15] states that, for small enough k, many of the original invariant curves will survive. These particular KAM curves can be characterized by their winding number W:

$$W = \lim_{n\to\infty} \frac{\theta_n - \theta_0}{n} \tag{1.4}$$

Greene,[8] in his extensive and pioneering studies of this map, has found empirically that the last remaining KAM curve with finite W has $W = (\sqrt{5} - 1)/2$, the reciprocal of the Golden Mean. This KAM curve disappears when k reaches the critical value of $k_c = 0.9716354\ldots$. We focus our attention on this particular KAM curve and study its structure for $k = k_c$. (There are also other equivalent KAM curves, e.g., at winding numbers $\pm W$ plus an integer.) We find that at k_c the curve has a scale-invariant structure and can be analyzed using scaling functions analogous to those introduced by Widom.[17]

In Section 2, we present a more detailed explanation of the Moser twist theorem and our version of a method, introduced by Greene, of studying KAM curves. We present our results in Section 3, and discuss the precision of our numerical work in an Appendix.

2. METHODOLOGY

2.1. The Moser Twist Theorem

Our basic computational tool is the Moser twist theorem,[15] which states sufficient conditions for a KAM curve to exist. Consider an unperturbed twist map

$$\begin{aligned} T_0 : \begin{bmatrix} s_n \\ t_n \end{bmatrix} &\to \begin{bmatrix} s_{n+1} \\ t_{n+1} \end{bmatrix} \\ s_{n+1} &= s_n \\ t_{n+1} &= t_n + s_n \end{aligned} \tag{2.1}$$

and the perturbed map

$$T_k:\begin{bmatrix} r_n \\ \theta_n \end{bmatrix} \to \begin{bmatrix} r_{n+1} \\ \theta_{n+1} \end{bmatrix}$$
$$r_{n+1} = r_n + kg(\theta_n) \tag{2.2}$$
$$\theta_{n+1} = \theta_n + r_n + kg(\theta_n)$$

The theorem states that for a "sufficiently irrational" winding number $W = s_0$, and sufficiently small k, there is a change of coordinates U: $(s,t) \to (r,\theta)$

$$r(t) = s + v(t)$$
$$\theta(t) = t + u(t) \tag{2.3}$$

where u, v are periodic such that the relation

$$T_0 = U^{-1} T_k U \tag{2.4}$$

holds on the line $s = W$. The precise statement of the irrationality condition is that there exist c greater than zero such that for all integers m, n

$$\left| W - \frac{n}{m} \right| > \frac{c}{m^{2.5}} \tag{2.5}$$

Relations (2.3) will form the basis of our numerical studies. By constructing the functions $u(t)$, $v(t)$, we will have found a parametrization of the KAM curve. We can find equations for $u(t)$ and $v(t)$ directly by combining equations (2.3) and (2.4):

$$u(t + W) - u(t) = v(t) + kg(t + u(t))$$
$$v(t + w) - v(t) = kg(t + u(t)) \tag{2.6}$$

2.2. Cycles

Finite length periodic cycles have rational winding numbers. In particular if $\theta_Q = \theta_0 + P$, $r_Q = r_0$ then $W = P/Q$. The Q-cycles are characterized not only by their winding number but also by their stability properties. In the linearized limit, deviations $\delta\theta_0, \delta r_0$ about a fixed point of T_k^Q are mapped into deviations $\delta\theta_Q, \delta r_Q$ by the tangent map of T_k^Q evaluated at the fixed point:

$$\begin{bmatrix} \delta r_Q \\ \delta\theta_Q \end{bmatrix} = M \begin{bmatrix} \delta r_0 \\ \delta\theta_0 \end{bmatrix}, \qquad M = \begin{bmatrix} \dfrac{\partial r_Q}{\partial r_0} & \dfrac{\partial r_Q}{\partial \theta_0} \\ \dfrac{\partial \theta_Q}{\partial r_0} & \dfrac{\partial \theta_Q}{\partial \theta_0} \end{bmatrix} \tag{2.7}$$

Since T_k, and therefore T_k^Q, is area-preserving, M has determinant one and the eigenvalues λ_1, λ_2 depend solely on the trace of M:

$$\lambda^2 - \lambda(\mathrm{Tr}\, M) + 1 = 0 \tag{2.8}$$

Following Greene, we define the residue R of a cycle as $R = \frac{1}{4}(2 - \mathrm{Tr}\, M)$. The invariant curves of M are conic sections and generically they determine the stability properties of the cycle. There are two distinct classes. If $\lambda_1 = \lambda_2^*$ $(0 \leqslant R \leqslant 1)$ the invariant curves are ellipses and initially small deviations remain forever bounded.[3] If λ_1 is real ($R \leqslant 0$ or $R \geqslant 1$) the invariant curve is a hyperbola and initially small deviations increase exponentially. The residue provides a convenient way of classifying cycles as elliptic or hyperbolic.

At $k = 0$, all trajectories with $W = P/Q$, P and Q being relatively prime integers, are actually cycles of length Q in which θ increases by P in the course of the cycle. There is a one-parameter family of such Q-cycles since θ_0 is arbitrary. The twist theorem tells us nothing about the fate of these families of Q-cycles for nonzero k. The Poincaré–Birkhoff fixed point theorem states that for nonzero k, there are only a finite number of such Q-cycles left. In fact, there are an even number of these cycles, half of them elliptic and half of them hyperbolic. For our particular map, Greene[8] has observed that for small enough k there are exactly two such cycles for every $W = P/Q$.

In general the residue of a Q-cycle will change as we vary k. If the residue passes through one from below, the original elliptic Q-cycle bifurcates, becoming hyperbolic. Associated with this bifurcation is the creation or destruction of two or more longer cycles. See Greene et al.[18] for an extensive discussion of bifurcations in area-preserving two-dimensional maps.

2.3. Approximation of KAM Curve

The only analytic techniques for studying KAM curves directly are perturbative ones which break down for k near k_c, which is exactly the regime we are interested in. Numerical techniques, while nonperturbative, have their own weaknesses. Finding a KAM curve entails searching for a trajectory which never repeats itself yet continues to fill in a smooth curve in the r, θ plane forever. Clearly no finite precision, finite time numerical approach could ever test these conditions.

[3] There are nongeneric cases where the linear analysis is not enough to ensure stability, such as $\lambda^3 = 1$ or $\lambda^4 = 1$.

Greene,[8] however, has introduced a method for studying KAM curves which involves finite cycles only. Suppose one is interested in studying a KAM surface with irrational winding number W. First, construct a series of rational approximants $W_i = P_i/Q_i$ which converge to W

$$W = \lim_{i\to\infty} W_i \tag{2.9}$$

Then, find the two Q_i cycles with winding number W_i. Greene presents strong evidence that the KAM curve can be determined from the accumulation set of the points of these Q_i cycles. Thus, the KAM curve exists if there exists a sequence of Q_i cycles which converges onto a smooth curve. We assume that all behavior of the cycles which persists in the limit $Q_i \to \infty$ reflects the true behavior of the KAM curve.

Greene also shows that the existence of the KAM curve is strongly connected with the stability properties of the Q_i cycles. We introduce two functions $R_i^e(k), R_i^h(k)$ as the residues of the elliptic and hyperbolic Q_i cycles at a given value of the perturbation parameter k. Greene's data indicate that

$$\lim_{i\to\infty} R_i^e(k) = \begin{cases} 0^+, & k < k_c \\ a & k = k_c \\ \infty & k > k_c \end{cases} \tag{2.10}$$

$$\lim_{i\to\infty} R_i^h(k) = \begin{cases} 0^- & k < k_c \\ -b & k = k_c \\ -\infty & k > k_c \end{cases} \tag{2.11}$$

where a, b are positive constants less than unity. This provides an extremely accurate way of determining k_c. It also shows that for $k \leqslant k_c$, the elliptic cycles remain elliptic as $i \to \infty$, i.e., there are no bifurcations.

Our approach will be slightly different from Greene's in that the main object of study will not be the KAM curve in the r, θ plane but rather the functions $u(t)$ and $v(t)$. We can use the approximating Q_i cycles to construct functions $u_{Q_i}(t), v_{Q_i}(t)$ which approximate $u(t)$ and $v(t)$. For the cycle of type $\alpha(\alpha = e \text{ or } h)$ with winding number W_i we can construct relations directly analogous to Equations (2.3).

We write the cycles in the form

$$\begin{aligned} \theta_n^\alpha &= t_n^\alpha + u_{Q_i,n}^\alpha \\ r_n^\alpha &= W_i + v_{Q_i,n}^\alpha \end{aligned} \tag{2.12}$$

where

$$t_n^\alpha = t_0^\alpha + nW_i \tag{2.13}$$

To achieve a smooth transition to the $i \to \infty$ limit, we define in analogy to Eqs. (2.3) functions $r_{Q_i}(t)$, $\theta_{Q_i}(t)$, $u_{Q_i}(t)$ and $v_{Q_i}(t)$ which reduce, respectively, to the values r_n^α, θ_n^α, $u_{Q_i,n}^\alpha$, and $v_{Q_i,n}^\alpha$ when t has the values given by Eqs. (2.13). Thus Eqs. (2.12) imply

$$\begin{aligned} \theta_n^\alpha &= \theta_{Q_i}(t_n^\alpha) = t_n^\alpha + u_{Q_i}(t_n^\alpha) \\ r_n^\alpha &= r_{Q_i}(t_n^\alpha) = W_i + v_{Q_i}(t_n^\alpha) \end{aligned} \tag{2.14}$$

In order to achieve a full definition of these functions we demand that $\theta_{Q_i}(t) - t$, $r_{Q_i}(t) - W_i$, $u_{Q_i}(t)$, and $v_{Q_i}(t)$ all be periodic functions of t with period one and that $u_{Q_i}(t)$ be an odd function of t. The oddness can be achieved by picking t_0^α to be zero for the elliptic cycle and $(2Q_i)^{-1}$ for the hyperbolic cycle. Then, the functions $u_{Q_i}(t), v_{Q_i}(t)$ are defined on an evenly spaced mesh of points $t_j = j/2Q, j = 1, 2, \ldots, 2Q$. Just as we assumed that the Q_i cycles would converge onto the KAM curve, we also assume that the functions $u_{Q_i}(t), v_{Q_i}(t)$ will converge to $u(t), v(t)$, when an appropriate set of approximating cycles is chosen and their length is taken to ∞.

In our work, we often find it convenient to deal with the u's in their Fourier transformed representation. That is, we write for the KAM trajectory

$$u(t) = \sum_{\omega=1}^{\infty} A(\omega) \sin 2\pi\omega t \tag{2.15}$$

and for the cycles

$$u_{Q_i}(t) = \sum_{\omega=1}^{Q_i} A^{Q_i}(\omega) \sin 2\pi\omega t \tag{2.16}$$

where the ω's are integers. Equation (2.16) then serves to define $u_{Q_i}(t)$ for all values of t.

There is a systematic way to determine the rational approximants W_i. Every irrational $W \in (0, 1)$ has a unique representation as a continued fraction[19]

$$W = \cfrac{1}{a_1 + \cfrac{1}{a_2 + \cfrac{1}{a_3 + \cdots}}} \equiv \langle a_1, a_2, a_3, \ldots \rangle \tag{2.17}$$

where the a_i are positive integers. Truncating this series at the ith term produces a rational number

$$W_i = P_i/Q_i = \langle a_1, a_2, a_3, \ldots, a_{i-1}, a_i, \infty \rangle \tag{2.18}$$

which closely approximates W. These W_i represent the optimal choice for rational approximants. The deviations $W_i - W$ alternate in sign as i increases, so the KAM curves are bounded above and below by the Q_i cycles.

The size of the a_i indicate the closeness of W to rationals. In this sense, the most irrational number would have $a_i = 1$ for all i. The resulting number is $W = (\sqrt{5} - 1)/2$, the reciprocal of the Golden Mean. For this number, the rational approximants W_i are given by

$$W_i = F_i / F_{i+1} \tag{2.19}$$

where F_i indicates the ith Fibonacci number.[4] Interestingly, Greene's study indicates that the KAM surface having the largest critical coupling has winding number $W^* = (\sqrt{5} - 1)/2$. Greene points out that this is to be expected, since the KAM proofs stress the degree of irrationality of winding numbers. In any case, we will focus our attention on this winding number.

2.4. Symmetries

In general, finding a Q cycle involves searching the entire r, θ plane. However, the standard map has a symmetry property called reversibility[20,18] which greatly simplifies this task. Reversibility implies that the standard map T_k can be written as a product of two involutions

$$T_k = I_2 I_1 \tag{2.20}$$

with

$$I_1 \begin{bmatrix} r \\ \theta \end{bmatrix} = \begin{bmatrix} r - (k/2\pi)\sin 2\pi\theta \\ -\theta \end{bmatrix}, \qquad I_2 \begin{bmatrix} r \\ \theta \end{bmatrix} = \begin{bmatrix} r \\ r - \theta \end{bmatrix} \tag{2.21}$$

Note that $I_2^2 = I_1^2 =$ identity map and $\det I_1 = \det I_2 = -1$.

Greene[8,18] has observed that for any Q cycle, at least two out of its Q points are fixed points of I_1 or I_2. Thus, to find a Q cycle, we need only search four lines in the r, θ plane

$$\begin{aligned} a &= \{(r,\theta) \mid \theta = 0\} \\ b &= \{(r,\theta) \mid \theta = 1/2\} && \text{fixed points of } I_1 \\ c &= \{(r,\theta) \mid \theta = r/2\} \\ d &= \{(r,\theta) \mid \theta = (r+1)/2\} && \text{fixed points of } I_2 \end{aligned} \tag{2.22}$$

Since each cycle must have two points in the union of these sets, a cycle starting at a point $z_0 \in a$ must eventually be mapped into one of the sets a,

[4] The Fibonacci numbers are defined by $F_0 = 0$, $F_1 = 1$, $F_{i+1} = F_i + F_{i-1}$.

Table I. Routing Patterns for Rational Approximants to $W = \langle 1111111 \ldots \rangle$

i	$W_i = P_i/Q_i$	Routing pattern
0	0/1	I
1	1/1	II
2	1/2	III
3	2/3	I
4	3/5	II
5	5/8	III
6	8/13	I
7	13/21	II
8	21/34	III

b, c, or d before returning to z_0. For $k = 0$ and a particular winding number $W = P/Q$, we find three cases

$$\text{I} \left\{ \begin{matrix} Q \text{ odd} \\ P \text{ even} \end{matrix} \right\} \begin{matrix} z_0 \in a \Rightarrow \left(T_k^{(Q+1)/2} z_0\right) \in c, & z_0 \in c \Rightarrow \left(T_k^{(Q-1)/2} z_0\right) \in a \\ z_0 \in b \Rightarrow \left(T_k^{(Q+1)/2} z_0\right) \in d, & z_0 \in d \Rightarrow \left(T_k^{(Q-1)/2} z_0\right) \in b \end{matrix}$$

$$\text{II} \left\{ \begin{matrix} Q \text{ odd} \\ P \text{ odd} \end{matrix} \right\} \begin{matrix} z_0 \in a \Rightarrow \left(T_k^{(Q+1)/2} z_0\right) \in d, & z_0 \in d \Rightarrow \left(T_k^{(Q-1)/2} z_0\right) \in a \\ z_0 \in b \Rightarrow \left(T_k^{(Q+1)/2} z_0\right) \in c, & z_0 \in c \Rightarrow \left(T_k^{(Q-1)/2} z_0\right) \in b \end{matrix}$$

$$\text{III} \left\{ \begin{matrix} Q \text{ even} \\ P \text{ odd} \end{matrix} \right\} \begin{matrix} z_0 \in a \Rightarrow \left(T_k^{Q/2} z_0\right) \in b, & z_0 \in b \Rightarrow \left(T_k^{Q/2} z_0\right) \in a \\ z_0 \in c \Rightarrow \left(T_k^{Q/2} z_0\right) \in d, & z_0 \in d \Rightarrow \left(T_k^{Q/2} z_0\right) \in c \end{matrix}$$

We call the pattern of these lines mapping into each other a routing pattern, and it remains invariant as k varies unless a bifurcation occurs. We will always be working with cycles that have not bifurcated, so we can use these three general routing patterns. Since there are two Q_i cycles for each i, there are a total of four points on the symmetry lines a, b, c, d. It turns out that there is one on each line, with the elliptic cycle always having a point on the a-line. Following Greene et al.[18] we call this the dominant symmetry line.

It should be noted that for $W^* = (\sqrt{5} - 1)/2$, the series of the rational approximants cycles among the three routing patterns (see Table I). This will be important in our subsequent analysis.

3. RESULTS

Equipped with these numerical techniques, we studied the metamorphosis of the KAM curve with winding number $W^* = (\sqrt{5} - 1)/2$ as k

varied from 0 to k_c. Our results will be presented in three sections: a graphical section, in which we look at the global properties of the KAM trajectory, and sections on scaling and universality in which we focus upon very restricted regions of the KAM curve.

3.1. Global Properties

When $k = 0$, the KAM curve is the straight line $r = W^*$ in the r, θ plane. Each approximating Q_i cycle has Q_i points equally spaced along the line $r = W_i$ (Fig. 1). Actually, there are an infinite number of such cycles for each i, filling in the entire line, but we have depicted only the two cycles that persist for nonzero k. These cycles clearly converge onto the KAM curve, and the rate of convergence δ is merely that of the rational approximants

$$\delta = \lim_{i \to \infty} \frac{W_{i+1} - W_i}{W_i - W_{i-1}} = -(W^*)^2 \tag{3.1}$$

For $k = 0.5$, the straight line becomes somewhat deformed. Figure 2a shows the two cycles with winding number $W_{18} = 2584/4181$. While this is not the exact KAM curve, it would be impossible to see any deviations on this graph since $|W_{18} - W^*| < 3 \times 10^{-8}$. A magnified view of a portion of these cycles reveals an essentially linear structure (Fig. 3a).

The critical case, $k = k_c$, is problematical. The 4181 cycles appear smooth (Fig. 2b) but all of their detailed structure is washed out by the poor resolution of the graphics. The magnified view (Fig. 3b) reveals a tremendous amount of fine-scale structure. It turns out that the critical Q_i

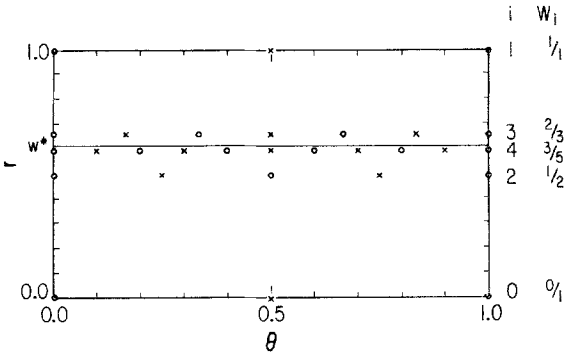

Fig. 1. Several approximating Q_i cycles converging onto the invariant curve $r = W^*$ (solid line) for $k = 0$. The O's (×'s) denote cycles which become elliptic (hyperbolic) for nonzero k.

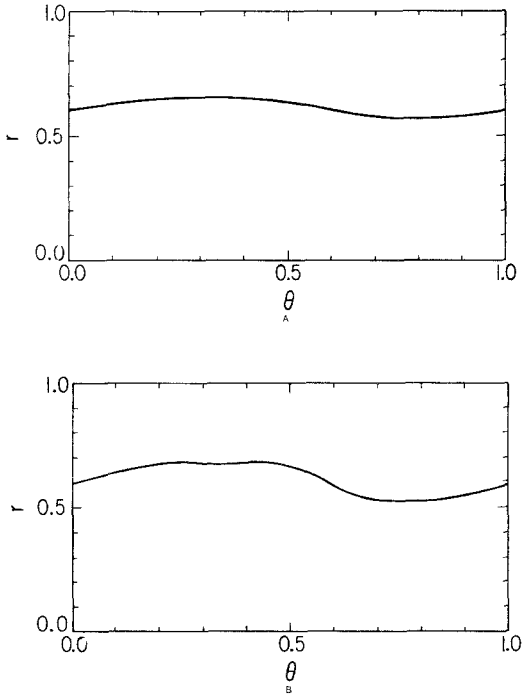

Fig. 2. The two cycles with winding number $W_{18} = 2584/4181$. In (a) $k = 0.5$ and in (b) $k = k_c = 0.9716354$. The finite resolution of the graphics turns the 8362 discrete points into a smooth curve.

cycles never have linear behavior on any length scale, and continue to exhibit finer and finer structure as i increases. Greene[8] presents pictures similar to these, and the reader is referred there for a more complete discussion.

We study the KAM curve through the functions $u(t)$ and $v(t)$. Actually, we need only study $u(t)$ since the two functions are simply related through relations (2.6)

$$v(t) = u(t) - u(t - W^*) \tag{3.2}$$

The function $u(t)$ represents deviations from integrable behavior so it is identically zero for $k = 0$. For $k = 0.5$, the magnitude of $u(t)$ is still quite small (Fig. 4a shows $u_{Q_i}(t)$ with $Q_i = 4181$). Only a few of the Fourier coefficients $A^{Q}(\omega)$ are large (Fig. 5a). We have plotted $\omega \times A(\omega)$ vs. ω so as to exhibit the high ω end of the spectrum more clearly. As k increases the magnitude of $u(t)$ grows roughly linearly in k, and there is a marked

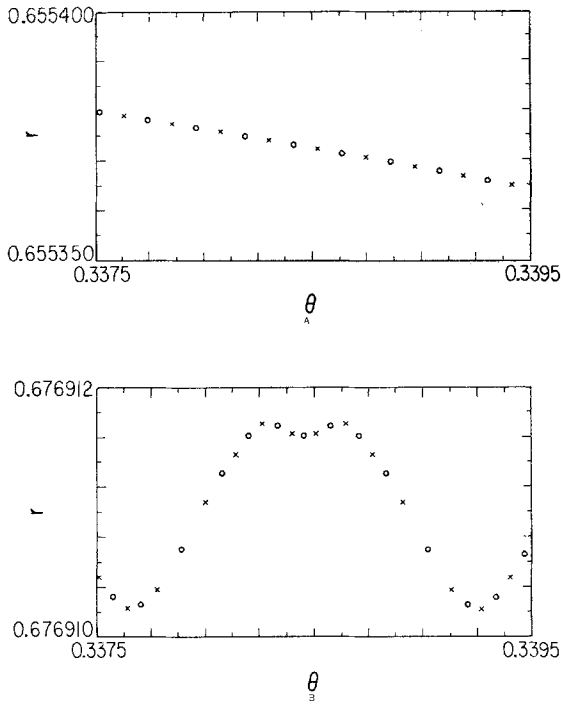

Fig. 3. Magnified views of a portion of the two cycles with winding number $W_{18} = 2584/4181$. In (a) $k = 0.5$ and in (b) $k = k_c = 0.9716354$. The ○'s (×'s) denote points on the elliptic (hyperbolic) cycle.

increase in the higher Fourier components (Figs. 4b and 5b). The primary peaks in the spectrum occur at Fibonacci numbers, reflecting the fact that the motion is almost periodic after F_i iterations. The subpeaks occur at sums and differences of nonadjacent Fibonacci numbers, which is again symptomatic of the almost periodic nature of the KAM curve. An empirical formula suggested by D. Escande[21] which captures much of this behavior is

$$A(\omega) \sim \frac{e^{-\beta(k)\omega}}{\omega^3 |\sin 2\pi\omega W^*|^2} \tag{3.3}$$

where $\beta(k)$ is a positive function of k. It should be stressed that while this form of $A(\omega)$ gives a reasonable representation of the largest peaks in the data, it does not yield quantitatively correct scaling behavior.

Figures 4c and 5c depict the critical $u(t)$ and its Fourier transform. Now the Fourier peaks decay algebraically (as $1/\omega$), not exponentially, so that $\beta(k_c) = 0$ in the above formula. By fitting the spectra to this functional form for several values of k near k_c it was determined that $\beta(k)$ is

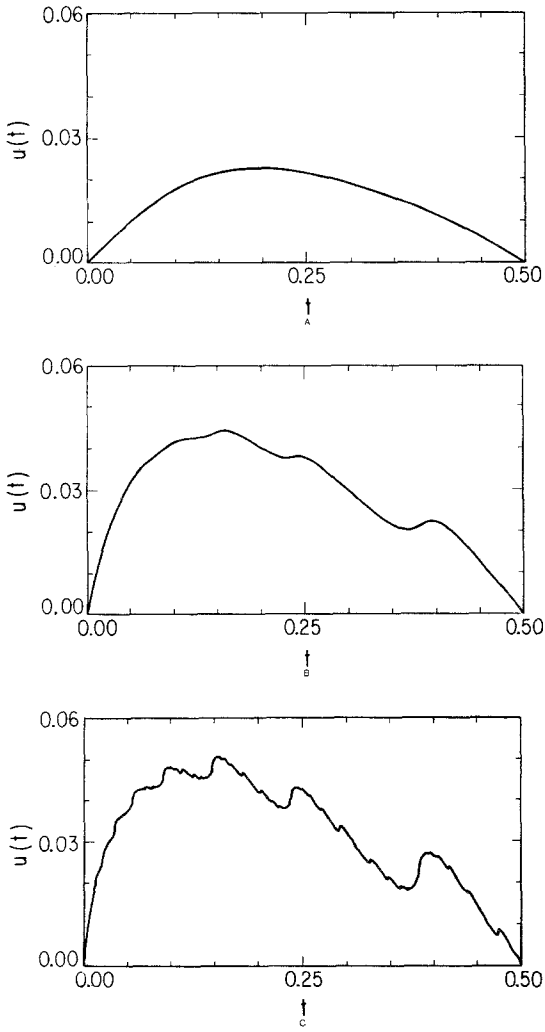

Fig. 4. The function $u_{Q_i}(t)$ for $Q_i = 4181$. In (a) $k = 0.5$, in (b) $k = 0.9$, and in (c) $k = k_c = 0.9716354$. Since we have chosen $u_{Q_i}(t)$ to be an odd function with unit period, we need only display the function for $0 \leqslant t \leqslant 0.5$.

essentially linear in $k_c - k$ for small deviations from criticality. It is clear from the form of $A(\omega)$ that while $u(t)$ is continuous for $k = k_c$, it lacks a continuous derivative. For example, the derivative at $t = 0$

$$u'(0) = \sum_{\omega} \omega A(\omega) \tag{3.4}$$

diverges.

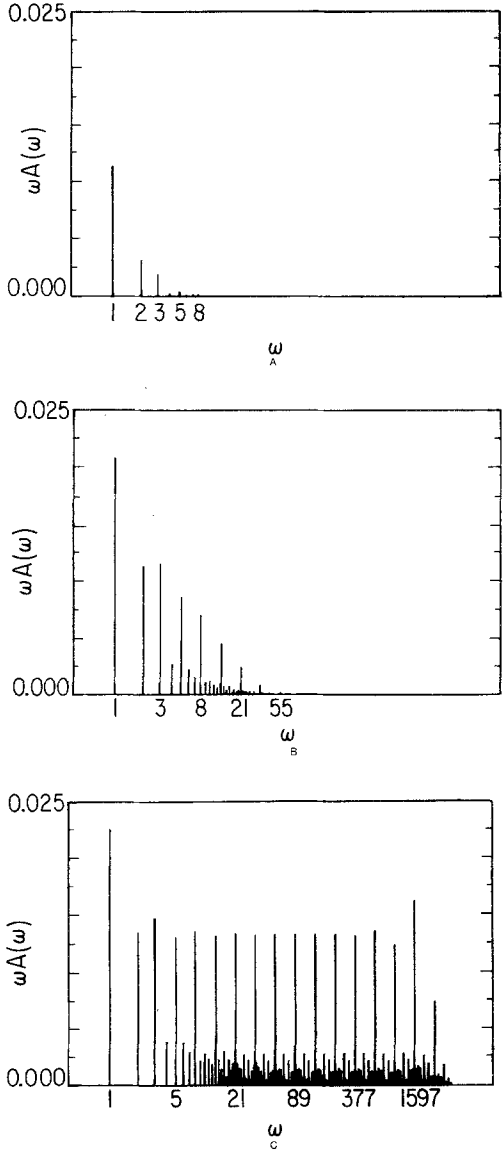

Fig. 5. The Fourier coefficients $A^{Q}(\omega)$ for $Q_i = 4181$. In (a) $k = 0.5$, in (b) $k = 0.9$, and in (c) $k = k_c = 0.9716354$.

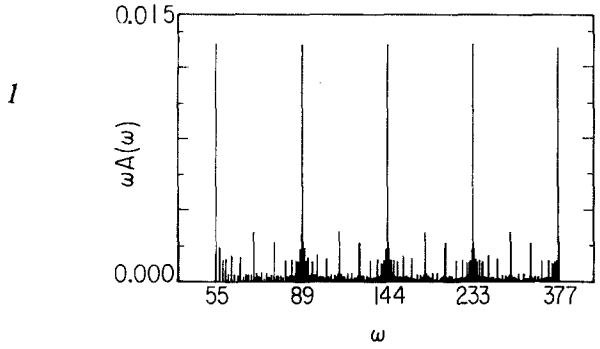

Fig. 6. The Fourier coefficients $A^{Q_i}(\omega)$ for $Q_i = 4181$, $k = k_c = 0.9716354$ and $55 \leqslant W \leqslant 377$.

We are now in a position to justify the claim that $u(t)$ at $k = k_c$ has "structure at all length scales." Consider Fig. 6, which is the spectrum $A^{Q_i}(\omega)$ for $k = k_c$ and $Q_i = 4181$ with the low and high ω behavior deleted. (The deviations from regularity for high ω are merely due to the finite size of the cycle, and would disappear in the limit $Q_i \to \infty$.) Between any two consecutive primary peaks there is a repetition of essentially the same complicated structure. Thus, the major features of structure in $A(\omega)$ for $Q_{i-1} \leqslant \omega \leqslant Q_i$ is almost the same as for $Q_i \leqslant \omega \leqslant Q_{i+1}$, except that the frequencies are scaled up by a factor Q_{i+1}/Q_i and the magnitudes of the Fourier components are scaled down by the same factor. The limiting result of this infinite cascade is a function $u(t)$ which has "structure at all length scales." Furthermore, we can posit the stronger statement that the structures at different length scales are similar and related. This leads to scaling.

3.2. Scaling

The scaling properties are best illustrated by investigating how the discrete functions $\theta_{Q_i}(t)$ converge to $\theta(t)$. The quantity of interest is $d_i(t)$, where

$$d_i(t) = \theta_{Q_i}\left(t + \frac{1}{2Q_i}\right) - \theta_{Q_i}(t) \tag{3.5}$$

is the difference in $\theta_{Q_i}(t)$ at two adjacent points. Numerical results indicate that for all $k \leqslant k_c$

$$\lim_{i \to \infty} d_i(t) = 0 \tag{3.6}$$

establishing the continuity of $\theta(t)$. For $k < k_c$, and sufficiently large i, the difference $d_i(t)$ becomes essentially linear in $(2Q_i)^{-1}$ and

$$\theta'(t) = \lim_{i\to\infty} \frac{d_i(t)}{(1/2Q_i)} \tag{3.7}$$

has a well-defined, finite limit.

At criticality, the difference $d_i(t)$ never becomes linear in $(2Q_i)^{-1}$. Instead, the deviation falls to zero via some nonanalytic power law. This is most easily seen at $t = 0$,

$$d_i(0) \sim Q_i^{-x_0} \tag{3.8}$$

where $x_0 = 0.721 \pm .001$. To present the results for nonzero t, we must remember that the routing patterns have period three. This fact, apparently unimportant below criticality, is crucial for analyzing the $k = k_c$ results; the observed power laws are apparent only when we shift i by three. For instance, the scaling behavior at $t = 1/2$ is

$$d_{3i+j}(\tfrac{1}{2}) \sim a_j Q_{3i+j}^{-x_1} \tag{3.9}$$

where $j = 0, 1, 2$, the a_j are constants, and $x_1 = 1.093 \pm .001$.

We can connect the critical and subcritical behavior through the use of scaling functions. All of our information about the scaling properties of $d_i(t)$ can be expressed in the two relations

$$\begin{aligned} d_i(0) &\sim Q_i^{-x_0} f_0\left(\frac{1}{\epsilon Q_i}\right) \\ d_{3i+j}(\tfrac{1}{2}) &\sim Q_{3i+j}^{-x_1} f_1^{(j)}\left(\frac{1}{\epsilon Q_i}\right) \end{aligned} \tag{3.10}$$

where $\epsilon = k_c - k$ and the scaling functions satisfy

$$\begin{aligned} &\text{(i)} \qquad f_0(\lambda) \sim \lambda^{1-x_0}, \qquad \lambda \ll 1 \\ &\qquad\qquad f_1^{(j)}(\lambda) \sim \lambda^{1-x_1}, \qquad \lambda \ll 1 \\ &\text{(ii)} \qquad \lim_{\lambda\to\infty} f_0(\lambda) \text{ and } \lim_{\lambda\to\infty} f_1^{(j)}(\lambda) \text{ exist and are finite} \end{aligned} \tag{3.11}$$

In Figs. 7 and 8 we exhibit the numerical evidence for the existence of the scaling functions $f_0, f_1^{(0)}$. Similar evidence exists for the other scaling functions $f_1^{(1)}$ and $f_1^{(2)}$. In Eqs. (3.10) a fit to a function of $\epsilon^{\nu} Q_i$ is also possible. Roughly equally good fits are obtained throughout the range $0.98 < \nu < 1.01$. However, for theoretical reasons (see below) it seems sensible to guess $\nu = 1$.

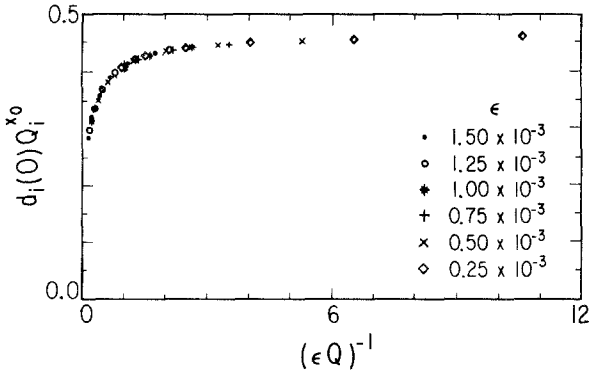

Fig. 7. Evidence for the existence of the scaling function $f_0(1/\epsilon Q_i) = d_i(0)Q_i^{x_0}$. $d_i(0)Q_i^{x_0}$ has been plotted versus $(\epsilon Q_i)^{-1}$ for several values of Q_i and $\epsilon = k_c - k$.

We now return to the r, θ plane and study how the Q_i cycles converge onto the KAM curve. In order to make quantitative statements we must restrict our attention to the intersection of the Q_i cycles with the a and b symmetry lines. Let r_i^a, r_i^b denote the values of r for the points on the Q_i cycles having $\theta = 0$, 0.5 respectively. Then, we study how these values converge to the limiting values

$$\begin{aligned} r_\infty^a &= \lim_{i\to\infty} r_i^a \\ r_\infty^b &= \lim_{i\to\infty} r_i^b \end{aligned} \tag{3.12}$$

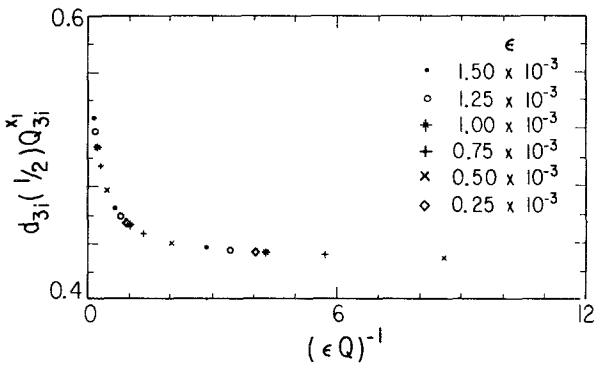

Fig. 8. Evidence for the existence of the scaling function $f_1^{(0)}(1/\epsilon Q_{3i}) = d_{3i}(1/2)Q_{3i}^{x_1}$. $d_{3i}(1/2)Q_{3i}^{x_1}$ has been plotted versus (ϵQ_{3i}) for several values of Q_{3i} and $\epsilon = k_c - k$.

which are the r values of the intersection of the KAM curve with the a and b symmetry lines. Numerical results show that for $k < k_c$, $\alpha = a$ or b

$$\frac{r_{i+1}^{\alpha} - r_i^{\alpha}}{r_i^{\alpha} - r_{i-1}^{\alpha}} \sim \left[\frac{Q_i}{Q_{i+1}} \right]^2 \tag{3.13}$$

indicating that $r_i^{\alpha} - r_{\infty}^{\alpha} \sim Q_i^{-2} \sim W - W_i$. This is exactly the convergence behavior we found in the integrable limit $k = 0$. It shows that the approximating Q_i-cycles are arranged linearly in $W^* - W_i$ around the KAM curve.

For $k = k_c$, the r_i^{α} approach r_{∞}^{α} in a nonanalytic fashion. Our numerical results indicate that

$$\frac{r_{i+1}^{a} - r_i^{a}}{r_i^{a} - r_{i-1}^{a}} \sim \left[\frac{Q_i}{Q_{i+1}} \right]^{y_0} \tag{3.14}$$

$$\frac{r_{3(i+1)+j}^{b} - r_{3i+j}^{b}}{r_{3i+j}^{b} - r_{3(i-1)+j}^{b}} \sim \left[\frac{Q_{3i}}{Q_{3(i+1)}} \right]^{y_1} \tag{3.15}$$

where

$$\begin{aligned} y_0 &= 2.329 \pm .001 \\ y_1 &= 1.957 \pm .001 \end{aligned} \tag{3.16}$$

This is consistent with

$$|r_i^{a} - r_{\infty}^{a}| \sim Q_i^{-y_0} \sim |W_i - W^*|^{y_0/2} \tag{3.17}$$

$$|r_{3i+j}^{b} - r_{\infty}^{b}| \sim b_j Q_{3i+j}^{-y_1} \sim b_j |W_{3i+j} - W^*|^{y_1/2} \tag{3.18}$$

where b_j is a set of constants. However, we cannot use scaling functions to combine the critical and subcritical behavior of r, because we have no independent method for determining r_{∞}^{α} to sufficient accuracy.

The tangent map also exhibits scaling behavior. Each tangent map $M_i(z_0)$ at a fixed point z_0 of $T_k^{Q_i}$ can be characterized by three quantities:

(i) Residue $R_i(z_0) = \frac{1}{4}[2 - \operatorname{Tr} M_i(z_0)]$
(ii) Ratio $\rho_i(z_0)$ of minor to major axes of the invariant curves (hyperbolae or ellipses) of $M_i(z_0)$
(iii) Tilt angle $\phi_i(z_0)$ of the major axis with respect to the θ-axis.

The tilt angle ϕ has the least interesting behavior. For all nonzero k, $\phi_i(z_0)$ has a finite nonzero limit $\phi(z_0)$ as $i \to \infty$. The ratios $\rho_i(z_0)$ have a far less trivial critical behavior, one that depends on the symmetry class of z_0. For fixed points z_0 on the a symmetry line

$$\rho_i(z_0) \sim Q_i^{-\eta_0} h_0\left(\frac{1}{\epsilon Q_i} \right) \tag{3.19}$$

and for z_0 on the b symmetry line,

$$\rho_{3i+j}(z_0) \sim Q_{3i+j}^{-\eta_1} h_1^{(j)}\left(\frac{1}{\epsilon Q_{3i+j}}\right) \tag{3.20}$$

where $\eta_0 = 1.608 \pm .001$, $\eta_1 = 0.864 \pm .001$ and the scaling functions $h_\alpha(\lambda)$ reach a finite limit at $\lambda = \infty$. Figures 9 and 10 present the evidence for the existence of the scaling functions $h_0, h_1^{(0)}$. Once again, similar evidence exists for the other scaling functions $h_1^{(1)}$ and $h_1^{(2)}$.

The residue $R_i(z_0)$ is invariant under coordinate transformations, depending only on the trace of $M_i(z_0)$, so the residue at any two fixed points of $T_k^{Q_i}$ on the same Q_i cycle will have the same residue. Thus, we need only consider the two functions R_i^e, R_i^h defined in Section 2. In the limit of large Q_i and small ϵ, the residues are matched quite closely by the formula

$$\begin{aligned} R_i^e &\sim R_\infty^e (W^*)^{\epsilon\beta_0 Q_i} \\ R_i^h &\sim R_\infty^h (W^*)^{\epsilon\beta_0 Q_i} \end{aligned} \tag{3.21}$$

where $R_\infty^e = 0.250 \pm .001$, $R_\infty^h = -0.255 \pm .001$, and $\beta_0 = 2.30 \pm .01$. If we had chosen the scaling index, ν, for ϵ to be different from unity then Eq. (3.21) would imply that for large Q and small ϵ, R^h would be a function of $\epsilon^\nu Q$. However, Greene has argued that for all $\epsilon < 0$ the residues have a leading behavior which is exponential in Q. Hence the only possible structure is $\ln R^h \sim \epsilon^\nu \beta_0 Q_i \ln W^*$. But since the hyperbolic cycles vary

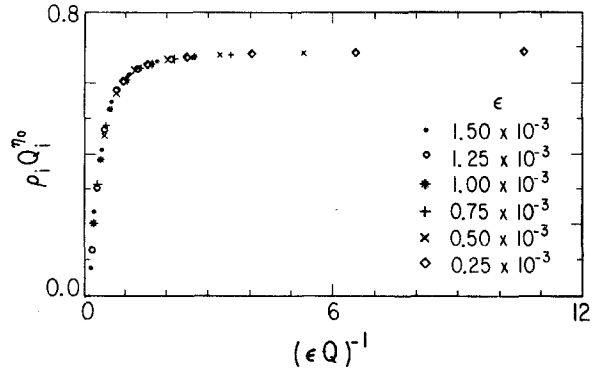

Fig. 9. Evidence for the existence of the scaling function $h_0(1/\epsilon Q_i) = \rho_i(z_0) Q_i^{\eta_0}$, where z_0 is a fixed point of T^{Q_i} on the $\theta = 0$ symmetry line. $\rho_i(z_0) Q_i^{\eta_0}$ has been plotted versus $(\epsilon Q_i)^{-1}$ for several values of Q_i and $\epsilon = k_c - k$.

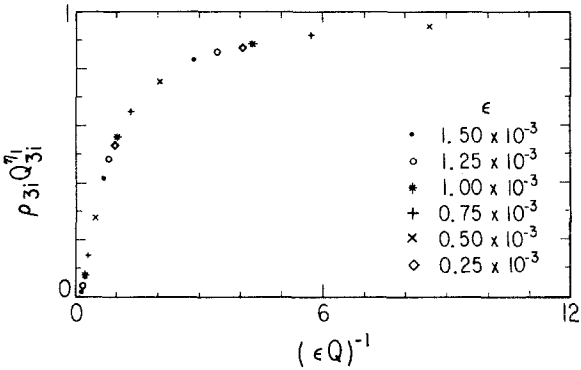

Fig. 10. Evidence for the existence of the scaling function $h_1^{(0)}(1/\epsilon Q_{3i}) = \rho_{3i}(z_0) Q_{3i}^{\eta_1}$, where z_0 is a fixed point of $T^{Q_{3i}}$ on the $\theta = \frac{1}{2}$ symmetry line. $\rho_{3i}(z_0) Q_{3i}^{\eta_0}$ has been plotted versus $(\epsilon Q_{3i})^{-1}$ for several values of Q_{3i} and $\epsilon = k_c - k$.

smoothly as ϵ passes through zero, it is unreasonable to assume any singularity in ϵ at $\epsilon = 0$ in R_i^h, for any finite value of i. We therefore argue that the only reasonable value of ν is $\nu = 1$.

In Ref. 6, Greene points out that for $k = 0.9$, the exponential damping coefficient for $A(\omega)$ is the same (to within $10^{-2}\%$) as the convergence rate for the residues. In our notation this implies that $\beta(k) = (k_c - k)\beta_0 \ln W^*$ holds at this value of k. Our data are consistent with this relationship holding to within 1% for all k close to k_c.

It is interesting to note that β_0 and y_0 are within a few per cent of each other. We do not yet know whether this is merely a numerical coincidence, or an indication of a rather deep relationship between the two scaling laws (3.10) and (3.21). There is another identity between exponents; to within numerical accuracy,

$$\eta_l = y_l - x_l \tag{3.22}$$

with $l = 0, 1$. This is easily explained since, for $\epsilon = 0$, the ratio ρ_i is proportional to the matrix element $\partial\theta_Q/\partial r_0$. Since θ scales as Q^{x_l} and r scales as Q^{y_l}, we would expect ρ to scale as $Q^{x_l - y_l}$.

We are left with two pairs of independent scaling exponents, x_l and y_l. The $l = 0$ pair describes scaling near $\theta = 0$, while the second pair describes the $\theta = 1/2$ scaling. One might expect the two scaling behaviors to be quite independent. Surprisingly, there is a nontrivial relationship between them,

$$x_1 + y_1 = \tilde{d} = x_0 + y_0 \tag{3.23}$$

with $\tilde{d} = 3.050 \pm .001$. This is a hint that perhaps the fundamental scaling entity has dimensions $r \times \theta$.

Table II. Compilation of Scaling Results

		Critical coupling	Scaling exponents				Asymptotic value of residue	
		k_c	x_0	x_1	y_0	y_1	Stable cycles	Unstable cycles
(0)	Standard map $W = \langle 111111 \ldots \rangle$	0.9716354 $\pm .0000003$	$0.721 \pm .001$	$1.093 \pm .001$	$2.329 \pm .001$	$1.957 \pm .001$	$0.250 \pm .001$	$-0.255 \pm .001$
(i)	Standard map $W = \langle 3141111 \ldots \rangle$	0.834365 $\pm .000001$	$0.72 \pm .01$	$1.09 \pm .01$	$2.33 \pm .01$	$1.96 \pm .01$	$0.25 \pm .01$	$-0.25 \pm .01$
(ii)	Standard map $W = \langle 2222 \ldots \rangle$	0.95744 $\pm .00001$	$0.72 \pm .01$	$1.10 \pm .01$	$2.34 \pm .01$	$1.96 \pm .01$	$0.23 \pm .01$	$-0.23 \pm .01$
(iii)	Nonstandard map[a] $W = \langle 1111 \ldots \rangle$	0.5351 $\pm .0001$	$0.72 \pm .01$	$1.09 \pm .01$	$2.33 \pm .01$	$1.95 \pm .01$	$0.25 \pm .01$	$-0.26 \pm .01$

[a] Map defined in Eq. (3.24).

3.3. Universality

We have found a very intricate scaling structure for a very specific problem; the Golden Mean KAM curve of the standard map. It is important to know how universal this scaling behavior is. We have studied three related problems and found similar scaling behavior in each one. Our results are summarized in Table II, and are discussed below.

(i) Standard Map with $W = \langle 3141111 \ldots \rangle$. As can be seen in Table II, the scaling exponents and asymptotic values of the residue were the same as before, to within numerical uncertainty. Furthermore, the coefficients a_j were also identical to within the error bounds. This is evidence that perhaps the scaling behavior depends only on the asymptotic character of the continued fraction representation of the winding number.

(ii) Standard Map with $W = \langle 222 \ldots \rangle$. Here, the exponents were apparently the same, but the asymptotic values of the residue and the coefficients a_j were different. The per cent differences in the coefficients went as high as 40% compared to a numerical uncertainty on the order of 2%. An important difference between this winding number and the Golden Mean is that the routing periodicity in this case is two (see Table III). This may be crucial in understanding the discrepancy in residues and coefficients.

(iii) Nonstandard Map with $W = \langle 1111 \ldots \rangle = W^*$. We studied the map

$$\begin{aligned} r_{n+1} &= r_n - \frac{k}{2\pi}\left[\sin 2\pi\theta_n + 0.01 \sin 6\pi\theta_n\right] \\ \theta_{n+1} &= \theta_n + r_{n+1} \end{aligned} \tag{3.24}$$

Table III. Routing Patterns for Rational Approximants to $W = \langle 222 \ldots \rangle = \sqrt{2} - 1$

i	$W_i = P_i/Q_i$	Routing pattern
0	0/1	I
1	1/2	III
2	2/5	I
3	5/12	III
4	12/29	I
5	29/70	III
6	70/169	I
7	164/408	III
8	408/985	I

and found identical values of the scaling exponents, residues, and coefficients a_j (Table II). It should be noted that the perturbation $-.01(k/2\pi)$ $\sin 6\pi\theta$ preserves all symmetries of the map.

Thus, in three closely related problems we found scaling exponents that agreed to within numerical uncertainty. It is fair to say that this indicates the existence of a "universality class" of problems which share this scaling behavior. We certainly do expect there to be other universality classes having quite different behavior.

APPENDIX

All of the numerical work was done in FORTRAN on a DEC-2050 computer using double precision (approximately 16 digits). Our study of the Golden Mean KAM curve involved Q_i-cycles whose length ranged from $Q_0 = 1$ to $Q_{21} = 17711$. A priori, one might expect the numerical error to be astronomical (on the order of $10^{-16} \times 2^{10^5}$), rendering the results meaningless. However, the internal consistency of our results provides some indication that numerical errors did not dominate our results.[5]

Using relations 3.8, 3.9, 3.14, and 3.15 we can compute a set of "apparent" scaling exponents at a given value of i using only data from Q_{i-1}, Q_i, and Q_{i+1} cycles. For $i = 8$ ($Q_i = 34$) all the exponents are within 1% of their final value. At this value of i, even the worst-case estimation of error leaves us with five significant figures. It appears that we can observe the scaling behavior in a regime where numerical errors are insignificant.

Furthermore, we have tested the effect of numerical error by adding a noise term into the recursion relations. The scaling results were essentially unchanged, although the convergence broke down for very large Q_i. For $i = 13$, $Q_i = 377$, the scaling exponents differed from the no noise result by less than $6 \times 10^{-4}\%$ and $6 \times 10^{-5}\%$ for the noise levels 10^{-12} and 10^{-14}, respectively. Furthermore, the residue values for both cases were within $5 \times 10^{-3}\%$ of the no noise result at $Q_i = 377$. Now, at this value of Q_i, the exponent values are within .001 (our quoted numerical uncertainty) of the final values. Thus we can argue that the scaling behavior we observe is not a product of our numerical error but is truly a manifestation of the properties of the standard map itself.

It should be noted that the numerical uncertainties quoted are merely

[5] Greene, in Ref. 8, shows that numerical errors tend to propagate along, not across, the KAM curve. It is not known whether this is responsible for the remarkable internal consistency of our data displays.

very conservative estimates of the internal consistency of our data, and in no way reflect an analysis of the error from first principles.

We have included, in Tables IV and V, a representative sample of our numerical data. Table IV lists the positive residue values for the standard map with three different values of k, and for the standard map with 10^{-14} noise and one value of k. Using Greene's conclusions about residues, Eq. (2.10), such data allow us to determine the value of k_c. Table V lists the apparent values of x_0 for the various cases. This apparent exponent is calculated via the formula

$$x_0^{(i)} = \frac{\ln\left[\dfrac{d_{i+1}(0)}{d_i(0)}\right]}{\ln W^*} \tag{A.1}$$

Table IV. Positive Residue Values for Cycles of the Standard Map with Three Different Values of k; $k = k_c - 10^{-4}$, $k = k_c$, $k = k_c + 10^{-4}$. Also Included are the Residue Values for Cycles of the Standard Map with a Noise Term of Magnitude 10^{-14} and $k = k_c$

		Standard map			Standard map with $10E^{-}14$ noise
I	Q	$K = 0.9715354$	$K = 0.9716354$	$K = 0.9717354$	$K = 0.9716354$
1	1	0.242884	0.242909	0.242934	0.242909
2	2	0.235970	0.236019	0.236067	0.236019
3	3	0.260599	0.260680	0.260761	0.260680
4	5	0.241889	0.242015	0.242141	0.242015
5	8	0.255306	0.255520	0.255734	0.255520
6	13	0.246271	0.246608	0.246946	0.246608
7	21	0.251738	0.252299	0.252861	0.252299
8	34	0.247821	0.248720	0.249623	0.248720
9	55	0.249462	0.250937	0.252421	0.250937
10	89	0.247184	0.249568	0.251975	0.249568
11	144	0.246526	0.250408	0.254352	0.250408
12	233	0.243617	0.249893	0.256331	0.249893
13	377	0.240059	0.250208	0.260788	0.250208
14	610	0.233719	0.250015	0.267454	0.250014
15	987	0.224143	0.250132	0.279158	0.250132
16	1597	0.209171	0.250059	0.299011	0.250055
17	2584	0.187041	0.250101	0.334639	0.250081
18	4181	0.155882	0.250072	0.401879	0.250087
19	6765	0.115953	0.250083	0.541916	0.250194
20	10946	0.071705	0.250066	0.883108	0.250027
21	17711	0.032889	0.250061	1.965774	0.257111

Table V. Apparent Exponent Values for Cycles of the Standard Map with Three Different Values of k; $k = k_c - 10^{-4}$, $k = k_c$, $k = k_c + 10^{-4}$. Also Included are the Exponent Values for Cycles of the Standard Map with a Noise Term of Magnitude 10^{-14} and $k = k_c$

		Standard map			Standard map with $10E^-14$ noise
I	Q	$K = 0.9715354$	$K = 0.9716354$	$K = 0.9717354$	$K = 0.9716354$
2	2	0.584152	0.584125	0.584098	0.584125
3	3	0.813029	0.812973	0.812917	0.812973
4	5	0.689105	0.689021	0.688937	0.689021
5	8	0.745081	0.744941	0.744800	0.744941
6	13	0.711971	0.711744	0.711516	0.711744
7	21	0.728624	0.728253	0.727882	0.728253
8	34	0.718536	0.717932	0.717326	0.717932
9	55	0.724460	0.723478	0.722493	0.723478
10	89	0.721556	0.719957	0.718350	0.719957
11	144	0.724544	0.721947	0.719328	0.721947
12	233	0.724907	0.720687	0.716411	0.720687
13	377	0.728259	0.721421	0.714433	0.721421
14	610	0.732020	0.720960	0.709505	0.720960
15	987	0.739034	0.721234	0.702384	0.721234
16	1597	0.749514	0.721064	0.689835	0.721063
17	2584	0.766009	0.721167	0.668904	0.721169
18	4181	0.790665	0.721106	0.632304	0.721091
19	6765	0.825410	0.721147	0.567350	0.721162
20	10946	0.869635	0.721128	0.451720	0.721141

REFERENCES

1. R. M. May, *Nature* **261**:495 (1976).
2. M. Feigenbaum, *J. Stat. Phys.* **19**:25 (1978); **21**:669 (1979).
3. P. Bak, *Phys. Rev. Lett.* **46**:791 (1981).
4. S. Aubry, in *Solitons in Condensed Matter Physics*, A. R. Bishop and T. Schneider, eds. (Springer Verlag, New York, 1978).
5. P. Collet and J.-P. Eckman, *Iterated Maps on the Interval as Dynamical Systems* (Birkhauser, Boston, 1980).
6. J. M. Greene, in *Nonlinear Dynamics*, R. H. G. Helleman, ed. (New York Academy of Sciences, New York, 1981), Vol. 357, p. 80.
7. J. M. Greene, *J. Math. Phys.* **9**:760 (1968).
8. J. M. Greene, *J. Math. Phys.* **20**:1183 (1979).
9. J. M. Greene and I. Percival, *Physica 3D* (1981).
10. R. G. Helleman, in *Fundamental Problems in Statistical Mechanics*, E. G. D. Cohen, ed. (North-Holland, Amsterdam, 1980), Vol. 5, p. 165.
11. M. V. Berry, in *Topics of Nonlinear Dynamics*, S. Jorna, ed. (AIP, New York, 1978), Vol. 46, p. 16.
12. B. Chirikov, *Phys. Rep.* **52**:265 (1979).

13. A. N. Kolmogorov, *Dokl. Akad. Nauk SSSR* **98**:527 (1954) (Russian).
14. V. I. Arnol'd, *Izv. Akad. Nauk* **25**:21 (1961).
15. J. Moser, *Nachr. Akad. Wiss. Göttingen Math. Phys. Kl.* **IIa**:1 (1962).
16. J. Taylor, unpublished (1968).
17. B. Widom, *J. Chem. Phys.* **43**:3989.
18. J. M. Greene, R. S. Mackay, F. Vivaldi, and M. J. Feigenbaum, *Physica 3D* (1981), 468.
19. I. Niven, *Irrational Numbers* (Mathematical Association of America, Menasha, Wisconsin, 1956).
20. G. D. Birkhoff, *Dynamical Systems* (AMS, New York, 1927).
21. D. Escande, Private communication (1981).